Structural properties of amorphous hydrogenated carbon. IV. A molecular-dynamics investigation and comparison to experiments

G. Jungnickel, Th. Frauenheim, D. Porezag, P. Blaudeck, and U. Stephan

Institute of Physics, Technical University of Chemnitz-Zwickau, D-09107 Chemnitz, Germany

R. J. Newport

Physics Laboratory, The University, Canterbury, Kent CT2 7NR, United Kingdom

Hydrogenated amorphous carbon structures, a-C:H, with densities of 1.8 and 2.0 g/cm^3, have been generated by semiempirical density-functional (DF) molecular-dynamics (MD) rapid cooling of a liquid phase of 128 carbon and 64 hydrogen atoms within periodically arranged cubic supercells. The electronic bonding properties of the model structures are analyzed within a local-orbital description. The structural properties are compared to relevant statistical and diffraction data obtained by neutron scattering and NMR in order to achieve a fundamental understanding of structure-related properties on the molecular level of chemical bonding.

I. INTRODUCTION

Theoretical structure simulations,[1-7] which are directly compared with experimental data,[8,9] have been established as a powerful tool for the experimental and theoretical understanding of the structural basis of material properties.[10] In this paper we investigate the structure-property relations in amorphous hydrogenated carbon modifications, a-C:H, with densities of 1.8 and 2.0 g/cm^3, as described in Ref. 11. The structural analysis in parts I–III of this series of papers[11-13] describes high-resolution neutron diffraction, inelastic neutron scattering studies, and NMR investigations. In order to achieve an insight into the atomic microstructure of the corresponding low-density a-C:H materials, atomic-scale simulations of a-C:H modifications with an incorporation of 33 at.% hydrogen and 1.8 and 2.0 g/cm^3 mass density have been performed.

II. MOLECULAR-DYNAMICS MODELING

In accord with the experiments[11-13] we have simulated amorphous hydrocarbon modifications by applying *semiempirical* density-functional molecular dynamics (DF-MD), which is described in more detail in Ref. 7. Within this method the total energy of the system is decomposed into two parts, $E_{tot}(\{\mathbf{R}_l\}) = E_{bind}(\{\mathbf{R}_l\}) + E_{rep}(\{\mathbf{R}_l - \mathbf{R}_k\})$. The first term appearing as the sum over all occupied cluster electron energies represents the so-called band-structure energy, and the second, as a repulsive energy, comprises all repulsive atom interactions. The latter are approximated by a short-range repulsive empirical two-particle potential that is fitted with respect to the self-consistent field local-density approximation (SCF LDA) potential energy curves of corresponding two-atomic molecules in dependence on a wide range of the interatomic separation. Examining carbon

microclusters,[14] fullerenes,[15] bulk crystalline and amorphous modifications, as well as diamond surfaces,[16] experimentally found structures are reproduced. Moreover, the relative differences of the cohesive energy per carbon atom as a function of structure and coordination closely approximate results obtained by more sophisticated methods.[17] As a proof, in Fig. 1 the cohesive energy for various carbon phases, diamond, graphite, carbyne, and body- and face-centered cubic modifications, is plotted versus interatomic distance. Though the short-range repulsive two-particle potential in Ref. 7 actually has not been fitted to these different carbon phases but to the two-atomic molecular data included in Fig. 1, the energetics of systems with varying coordination is correctly reproduced. These facts imply the energetically correct description of different pathways out of nonequilibrium initial configurations up to the formation of final metastable systems. A more detailed discussion of the
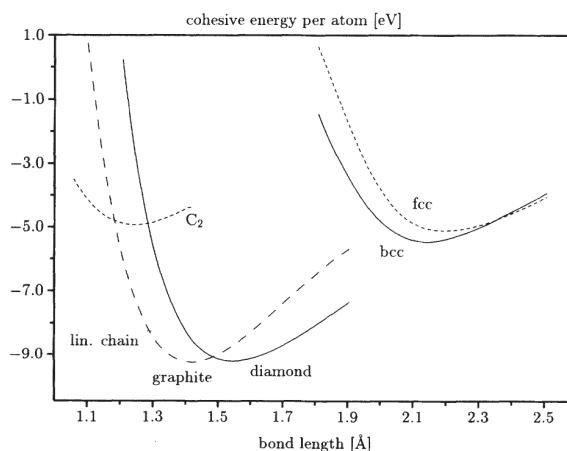

FIG. 1. Cohesive energy versus next neighbor distance for various carbon phases.

<u>50</u>   6709

transferability of the *semiempirical* DF scheme used to phases of varying coordination, finite systems, and different atom-type combinations will be given elsewhere.[18] The simulations have successfully been applied to study the stability and structure-property correlations in high- and low-density amorphous carbon, a-C.[9,19] In this work we present results of MD simulations carried out for periodic cubic supercells containing a fixed number of 128 carbon and 64 hydrogen atoms. The models to be investigated incorporate 33 at.% hydrogen and have been generated by the application of identical simulated annealing conditions, described in Ref. 7, cooling a partly equilibrated liquid over a total annealing time of 7×10^{-12} s.

III. STRUCTURE AND CHEMICAL BONDING

The microscopic mass density of the simulated structures and the hydrogen content strongly control the chemical bonding in the atomic configurations finally obtained. In Table I the mass densities and global chemical bonding parameters, along with some characteristic structure data, are given for the two models generated, in comparison with the experimental results taken from Refs. 11–13, hereafter referred to as Papers I, II, and III. The data include sp, sp^2, and sp^3 content, mean C-C bond length, mean C-C-C bond angle, and ring statistics.

To gain a deeper understanding of the chemical bonding properties in the amorphous hydrocarbon structures and the creation of defect states (i.e., dangling bonds), we have investigated the π-bonding character of our structures in a more quantitative manner using a simplified model.[20] A fourfold coordinated atom is conventionally referred to as being sp^3-like. Two lower coordinated atoms may be referred to as π bonded if the overlap integral of their free p hybrids exceeds a critical value necessary to create a significant minimum in the local density of states (LDOS) at an isolated pair of such atoms. The free orbitals not contributing to π bonds will be classified according to their p characters; they are considered as p-like if the p character of these hybrids is greater than a certain value. In this way, we can estimate the number of bonding and antibonding π states and the number of nonbonded p orbitals of the structures. Additionally, we can perform a search for strongly π-bonded atom groups

(referred to as "clusters" hereafter) including more than two atoms. A coarse estimate for the shape of the total electronic density of state (TDOS) near E_F may then be inferred from the ratio of the nonbonding p to the bonding and antibonding π states, n_p/n_π, and the ratio of $p + \pi$ states to the σ bonding and antibonding states, $n_{p+\pi}/n_\sigma$, given in Table I. The latter ratio is comparable to the ratio of the number of π bonds to σ bonds as was determined in Paper I regarding the number of π and σ states involved in these bond types. The first is a measure of the number of p defects influencing the gap region in the total density of states (TDOS). From Table I we conclude that the examined models are characterized electronically by a π-π^* gap behavior; the number of defects that would result in a finite DOS at the Fermi level is very small.

The most interesting fact is that the models contain a relatively large amount of twofold coordinated carbon atoms which could not be considered in the structural discussions of Papers I–III.[11–13] However, the inclusion of these species seems to be important in achieving a good agreement with the experimental results, as will be demonstrated in Sec. IV. The models are mainly composed of two- and threefold coordinated carbon atoms, whereas the fraction of fourfold coordinated sites does not exceed 30%.

The a-C:H structures of the densities considered show a less pronounced tendency to the formation of small rings than do the inorganic carbon allotropes. The number of rings with less than seven members per C atom is ≈ 0.22 for both models, which is lower than in diamond (2.0), graphite (0.5), and C_{60} (0.53). The major reason for this is the fact that the hydrogen atoms terminate network paths, which partly prevents the carbon atoms from building closed loops in the network. Additionally, in the initial steps of the relaxation this is associated with a tendency to generate small chainlike segments as precursor clusters which for atom numbers ≤ 5 are more stable than corresponding ring clusters.[14] We find that differently hybridized carbon atoms tend to cluster. Although π bonding is the main source for such cluster effects, the five-, six-, and seven-membered rings are strongly cross linked by the inclusion of at least one or two fourfold coordinated atoms and are thus not aromatic. Only in model 2 do we find one completely sp^2-bonded five-membered ring forming strong π bonds.

TABLE I. Structure and electronic bonding data for the a-C:H models, in comparison with experimentally determined values. NS indicates neutron scattering.

Analyzed structure	ρ (g cm^{-3})	$sp + sp^2$ (%)	sp^3 (%)	Mean C-C bond length (Å)	Mean C-C-C bond angle (deg)	Number of rings 4	5	6	7	n_p/n_π	$n_{p+\pi}/n_\sigma$
Sample 1 (NMR)	1.8	59	41								
Sample 1 (NS)	1.8	75	25	≈ 1.47[a]	≈ 118[b]						0.277
Sample 2 (NS)	2.0	81	19	≈ 1.47[a]	≈ 117[b]						0.294
Model 1	1.8	21+54	25	1.45±0.09	117.6±16.1	3	9	8	9	0.060	0.274
Model 2	2.0	16+56	28	1.47±0.09	116.6±14.7	0	15	5	8	0.047	00.241

[a]Mean C-C bond length obtained from the peak positions and areas in $G(R)$ (Paper I).
[b]Mean C-C-C bond angles derived from the relative C-C peak positions in $G(R)$.

However, the latter remains nonaromatic as is also observed for the other π-bonded clusters due to their embedding into a strained bonding environment. Separated aromaticlike ring groups that are broadly discussed in the literature as responsible for the small electronic band gaps in these materials have not been formed under the constraint of a cross-linked rigid network even at the low mass densities considered in the present simulation. The sp^2 atoms are rather arranged in olefinic groups as will be supported by the discussion of coordination numbers from experiment and theory in Sec. IV.

The bond length statistics of the models, shown in Fig. 2, are clearly subdivided into nonoverlapping groups from H-H, C-H, and C-C bonds as is expected from basic chemical considerations. Moreover, the carbon-carbon bonds are further subdivided into two groups containing different types of π bonds centered at positions typical for carbon triple and double bonds and a group with bond lengths longer than 1.43 Å which is typical for carbon single bonds (i.e., bonds with very low or no π character). The last group incorporates bonds between fourfold coordinated sites only $(sp^3$-$sp^3)$ and between threefold coordinated ones $(sp^2$-$sp^2)$ as well as "mixed" bonds $(sp^2$-sp^3, sp-sp^3, and sp-$sp^2)$ between differently coordinated atoms. The π-bonding groups arise from the clustered sp- and sp^2-like atoms forming bonds hereafter referred to as "double bonds" due to the interaction of lone p-like orbitals on neighboring sp- and sp^2 sites and "triple bonds" related to pairs of sp sites contributing two p electrons to the common σ bond. According to chemistry the largest bond lengths correspond to sp^3-sp^3 single bonds, whereas the shortest carbon bonds are related to the triple bonds.

IV. COMPARISON BETWEEN EXPERIMENT AND THEORY

As is demonstrated in Paper I of this series, the structure-related scattering from a multicomponent system arises from a superposition of weighted partials that are due to the different atom pairs occurring in the system. The weighting factors depend on the scattering properties of the atoms and their concentrations. In the theoretical procedure one has to determine the partial pair correlation functions and from that, via Fourier transformation, the partial structure factors. The superposition of these partials gives the total functions relevant for comparison with the experimental data. The partial pair correlation functions are calculated from the histograms of pair distances which can easily be generated from the models knowing the exact atomic positions. Moreover, the well-known atomic neighborhood in the theoretical models allows one to subdivide the total pair correlation function into components that reflect the network character of the structure, and into contributions from the different hybrids to the scattering data. Pairs of atoms can be indicated by the difference of their spatial vectors as well as their network distances k along σ bonds. Pair correlations $T^k(R)$ between first, second, third, and fourth σ-bonded neighbors $(k = 1, ..., 4)$ are separated here, while the other path lengths are incorporated into a joined fifth separated distribution function. The sum over the $T^k(R)$ yields the total path-separated radial distribution function $T(R)$ which is related to $J(R)$ (see Paper I) by $T(R) = J(R)/R$ and is used here for plotting convenience.
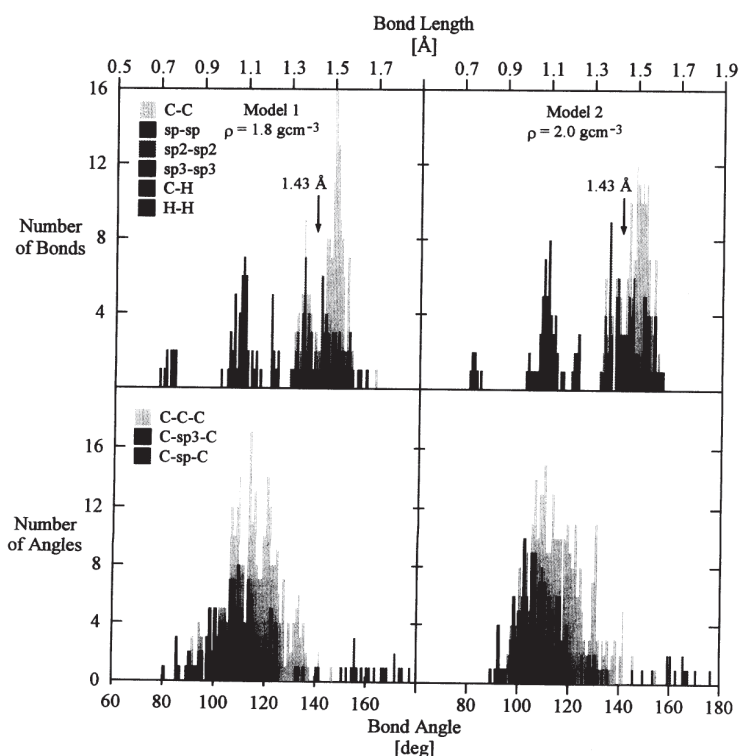

FIG. 2. Histograms of bond lengths and bond angles for the two model structures.

Analogously, a subdivision into hybrid contributions $H^k(R)$ is possible. In this case the index k no longer describes path length, but is rather used as an index for the hybridization state of each atom in the currently counted atomic pair. The sum of the partials $H^k(R)$ again yields a total curve $H(R)$ which is identical with $T(R)$.

From Table I it is apparent that the decrease of the mass density is associated with a decrease in the content of fourfold coordinated sites accompanied by a growing fraction of *sp*-like carbon species, which yields a lowering in the network connectivity and results in the formation of a more inhomogeneous carbon network. From the shortest path ring statistics according to a method proposed by Franzblau[21] and given in Table I, we find that an increase of the mass density yields a decrease of even-membered rings and favors the generation of five-membered rings. The total structure factors of the models (see Fig. 3) are in very good agreement with the experimentally determined scattering result. The height difference of the peaks at low momentum transfer is, however, an indication of the differences in the network connectivity of the models, and, due to contributions from intermediate-range correlations, of the tendency towards inhomogeneity mentioned above. Comparing the simulated structure factor with the neutron scattering data from samples deposited by a saddle-field ion beam technology described in detail in Paper I, one finds a difference in the positions of the first two sharp diffraction peaks. Moreover, the width of the first peak is not consistent for model 1 compared to sample 1. As is discussed in Paper I this may partly be due to problems arising from the inelasticity corrections. On the other hand, the limited supercell size in the theoretical procedure influ-

ences the structure factor in the same region, too. However, the remaining parts of the total structure factors are quite well represented by the two models.

Therefore the total pair correlation functions presented in Fig. 4 agree very well with the experimental results. In detail, we find all the peaks and shoulders assigned in Paper I to typical correlations that should occur in *a*-C:H. This is a pleasing result with respect to the complex influences on $G(R)$, where the peaks for the multicomponent system are due to the superposition of the atomic pair contributions as well as to an overlap of parts related to the true neighborhood as will be discussed later. Moreover, Fig. 4 shows that there is a subdivision of the first C-C correlation sphere into components centered at $R = 1.34$ Å and around $R = 1.51$ Å, as is found in the experiments. Differences between the theoretical and experimental curves are mainly found for peaks related to atomic correlations involving hydrogen atoms. This is particularly true for the H-H correlation sphere at $R \approx 0.87$ Å which is probably largely influenced by truncation effects and/or by the strong incoherent scattering of hydrogen during the neutron scattering experiment. The height of the H-H peaks determined in the experiment is inconsistent with the weak contribution of the simulated partial H-H pair correlation function (a concern supported by the small appropriate weighting factor W_{HH} which is ten and six times lower than the weightings for the C-C and C-H pair correlation functions, respectively).

Table II summarizes the peak positions in $G(R)$ for the models in comparison with the appropriate values determined by the experiments. If we use the clear drop in the bond length statistics at 1.43 Å (compare Fig. 2) as
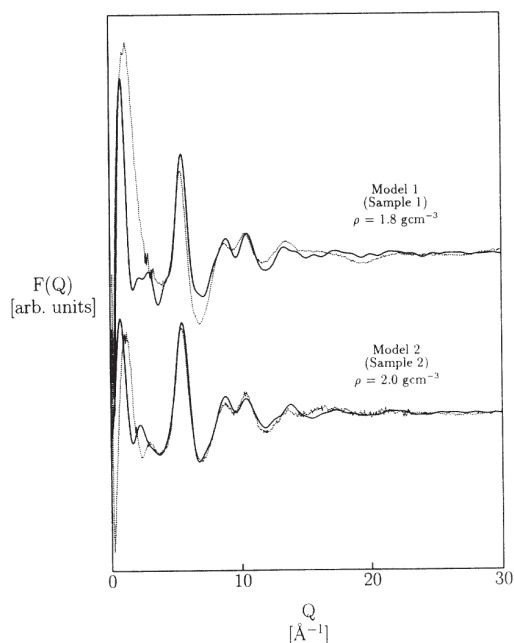

FIG. 3. Total structure factor $F(Q)$ for the generated *a*-C:H models compared with the neutron diffraction data of Paper I.
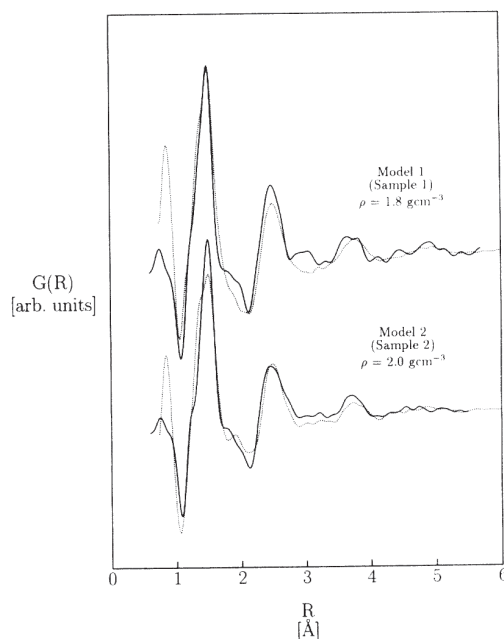

FIG. 4. Total pair correlation function $G(R)$ for the generated *a*-C:H models compared with the neutron diffraction data of Paper I.

TABLE II. Comparison of experimentally determined peak positions in $G(R)$ with data obtained directly from the bond length statistics and from the theoretical pair correlation functions of the two model structures.

Assignment (see Paper I)	Sample 1 $\rho=1.8$ g cm^{-3}	Sample 2 $\rho=2.0$ g cm^{-3}	Model 1 $\rho=1.8$ g cm^{-3}	Model 2 $\rho=2.0$ g cm^{-3}
H-H	0.88	0.86	0.74[a]	0.75[a]
C-H and H-C	1.03	1.06	1.07[a]	1.08[a]
$C\overset{(-)}{=}C$	1.34	1.34	1.34[a]	1.36[a]
C-C	1.52	1.53	1.51[a]	1.51[a]
H-C-H and C-C-H	1.7–2.2	1.7–2.2	1.82[b] 2.16[b]	2.00[b] 2.15[b]
C-C-C	≈ 2.5	≈ 2.5	2.49[b]	2.49[b]
C-C:$C\overset{(-)}{=}C$ ratio	2.6:1	2.4:1	2.0:1[a]	2.4:1[a]

[a]Mean values derived from bond length statistics.
[b]Peak position determined from $g_{\alpha\beta}(R)$.

a boundary between single (σ) and multiple (π) bonds, we obtain mean bond lengths for these particular types of bonds that are in very good agreement with the positions of the appropriate Gaussians derived by a fit to $G(R)$ determined using the neutron scattering data. Additionally, counting the carbon bonds in these groups yields a ratio between single and multiple bonds which agrees very well with the experimentally derived values in Paper I. The positions of the diverse second correlation spheres can be determined in the theoretical procedure by analyzing the partial pair distribution functions; these agree with the approximate values obtained from the experimental analysis of the total curves (see Table II). The mean C-C bond length and the mean C-C-C bond angle as well as their standard deviations, as given in Table I, also agree with the values obtained from the peak positions of the first two C-C correlation spheres in $G(R)$ within the uncertainties for such an approximation.

Amorphous hydrogenated carbon is characterized by local deviations from the symmetric atomic environment typical for the carbon allotropes and many organic hydrocarbon molecules. A description in terms of hybrids is only approximate and in a first step one should use a network-related description of the models. A method commonly applied is to define mean coordination numbers. For the models examined here, the coordination numbers $N_{\alpha\beta}$ result simply from the composition:

$$N_{HC} = 1 - N_{HH}, \qquad N_{CH} = \frac{x_H}{x_C} N_{HC}, \qquad (1)$$

$$N_{CC} = 4\{sp^3\} + 3\{sp^2\} + 2\{sp\} - N_{CH}, \qquad (2)$$

where N_{HH} is the relative number of hydrogens involved in H_2 molecules, x_C and x_H are the concentrations of carbon and hydrogen atoms in a given model, and $\{sp^3\}$, $\{sp^2\}$, and $\{sp\}$ are the fractions of the differently coordinated carbon atoms relative to their total sum.

The coordination numbers $N_{\alpha\beta}$ are directly related to the partial radial distribution functions. They can be obtained by integration of the first correlation shells of the appropriate partials. However, it is difficult to compute them from the total curves obtained in a single scattering experiment; the integrals taken over these total functions yield numbers that are weighted superpositions of the true coordination numbers. As is demonstrated by Table III for the models it is possible to compute the true coordination numbers with a relatively small error of 5–6 % from the integrals over the total radial distribution functions. For this we assume that the overlap of the partial radial distribution functions in the integration regions may be neglected, as is supported by the separation of the radial distribution in hybrid contributions, which is presented in Fig. 6 below. The integrals then have to be corrected for the weighting coefficients. The appro-

TABLE III. Coordination numbers derived from the radial distribution functions with the assumptions made in the text compared to the true numbers obtained from model composition.

Atomic correlations detected	Sample 1 $\rho=1.8$ g cm^{-3} from $T(R)$	Sample 2 $\rho=2.0$ g cm^{-3} from $T(R)$	Model 1 $\rho=1.8$ g cm^{-3} from $T(R)$	Model 1 as defined	Model 2 $\rho=2.0$ g cm^{-3} from $T(R)$	Model 2 as defined
H-H	2.33	2.89	0.30	0.31	0.22	0.22
C-H	0.42	0.81	0.29	0.24	0.34	0.31
H-C	0.77	1.51	0.58	0.69	0.68	0.78
C-C (total)	3.08	3.11	2.65	2.79	2.73	2.82
$C\overset{(-)}{=}C$ (multiple)	0.87	0.85	0.82	0.80	0.68	0.76
C-C (single)	2.21	2.26	1.83	1.99	2.05	2.06

priate results for the experimentally examined samples and the models are summarized in the Table III. With the exception of N_{HH} the coordination numbers for the models and the samples agree very well. This is particularly true for the multiple and single bond contributions in the total C-C correlation. These values are obtained by again using 1.43 Å as an integration boundary. The so-called "as defined" values in these cases come from the following approximation:

$$N_{CC}^{single} = 4\{sp^3\} + 2\{sp^2\} + r\{sp\} - N_{CH}, \qquad (3)$$

$$N_{CC}^{multiple} = \{sp^2\} + (2 - r)\{sp\}, \qquad (4)$$

e.g., every sp^2-like atom is assumed to contribute on average to one double bond (defects are neglected). Furthermore, any sp-like carbon atom can generate either two double bonds or one single and one triple bond. This variation is taken into account by the correction r, which is the relative number of sp-like atoms involved in triple bonds (0.74 for model 1 and 0.8 for model 2). This approximation yields a very good agreement with the results obtained from the integration. Therefore the experimental result that the threefold coordinated carbon atoms are probably arranged in olefinic groups rather than in aromatic rings is strongly supported. However, using the definitions for N_{CC}^{single} and $N_{CC}^{multiple}$ the ratio between these coordination numbers yields a complex relation between the fraction of sp^3-like and sp^2-like carbon atoms because of the inclusion of the twofold coordinated carbons:

$$\{sp^3\} = \frac{(2 - r) + A(N_{CH} - r)}{A(4 - r) + (2 - r)}$$

$$- \{sp^2\} \frac{(2 - r) + A(2 - r) - 1}{A(4 - r) + (2 - r)}, \qquad (5)$$

where A is the ratio between the area of the subpeaks in $G(R)$ centered at $R = 1.34$ Å and $R = 1.51$ Å, respectively.

Now we will concentrate on the distribution of the hydrogens. Using inelastic neutron scattering (INS), infrared-absorption measurements (Paper II), and nuclear magnetic resonance (Paper III), it is found from the experimental characterization that the majority of the hydrogen is strongly attached to sp^3-like carbon arranged in sp^3-H and sp^3-H$_2$ groups. Whereas these groups have equal fraction as determined by the different experiments, the amount of other C-H$_n$ groups is found to be higher in the NMR investigation than in the INS experiment. As is demonstrated in Table IV our two models correspond better with the NMR results. However, the fraction of sp^3-H$_2$ groups is considerably lower than in the experiments. This is probably due to a simulation regime that does not describe the true growth process. In the quench from a quasiliquid phase H$_2$ molecules can easily be generated. Therefore these hydrogens will no longer contribute to the formation of the hydrogenated network. In particular, they cannot contribute to a complete saturation and rehybridization of sp^2 sites that already are singly hydrogenated. If atomic hydrogen is present in such a model environment, as would be realistic for a growing surface, an addition of a second hydrogen atom to a monohydrogenated sp^2 atom causing rehybridization is highly favored. In this way the fraction of H$_2$ molecules, as well as the fraction of sp^2-H groups, would be reduced to increase the number of sp^3-H$_2$ radicals. The promotion of sp^3-like carbon then would be in better agreement with the NMR findings (see Table I).

Figures 5 and 6 show the separation of the (reduced) radial distribution function into contributions from the different neighbors (Fig. 5) and from diverse bonding situations (Fig. 6). From Fig. 5 it is apparent that the first H-H, C-H, and C-C correlation spheres are not influenced by higher order neighbor spheres. This is no longer the case for the second correlation spheres, which have contributions from several higher order neighbors. However, the figure shows that the situation is not as dramatic as in hydrogen-free high-density amorphous carbon systems.[9] In the present a-C:H analysis, the peak position of the second C-C correlation sphere is not shifted relative to the true correlation of second σ-bonded neighbors as it is in high-density a-C. Therefore it is possible to approximate the mean C-C-C bond angle from the position of the first C-C peaks in $G(R)$. However, an integration of the total radial distribution function using the boundaries of the second C-C correlation sphere clearly would yield too low second coordination numbers. It is interesting to note that for the systems investigated during this series of papers the influence of the distribution of fourth neighbors is almost fully compensated by higher order neighbor correlations in the range $R \leq 4$ Å. The peaks and shoulders between the second and third C-C correlation spheres in the total radial distribution func-

TABLE IV. Amount of several hydrogenated carbon environments (relative to carbon fraction) and of hydrogen molecules (relative to hydrogen fraction).

Types of H Bonds	Sample 1 (NMR) $\rho=1.8$ g cm^{-3}	Sample 1 (INS) $\rho=1.8$ g cm^{-3}	Sample 2 (INS) $\rho=2.0$ g cm^{-3}	Model 1 $\rho=1.8$ g cm^{-3}	Model 2 $\rho=2.0$ g cm^{-3}
sp^3-H$_2$	0.14	0.10-0.13	0.09-0.11	0.02	0.04
sp^3-H	0.09	0.08-0.10	0.08-0.10	0.12	0.11
other C-H$_n$	0.12[a]	< 0.05	< 0.05	0.17	0.16
H$_2$	found	found	found	0.31	0.22

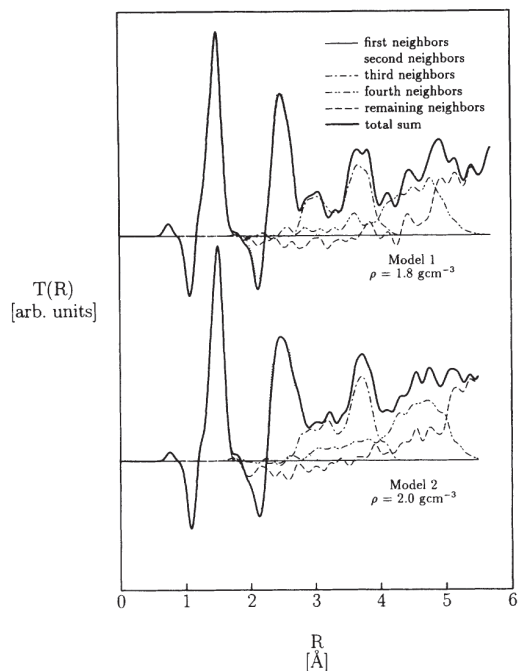[a]Using NMR only sp^2-H groups were detected.

FIG. 5. Network path separation of the radial distribution functions for the two a-C:H models.

tion are, therefore, a good measure of the distribution of third neighbors, which is directly related to the dihedral angle distribution of the system. The drop of this distribution at $R \approx 3.3$ Å depends strongly on the "mixed" C-C bonds as is shown in Fig. 6, whereas pure sp^2-sp^2 bonds only produce a flat background in this region. Fig-
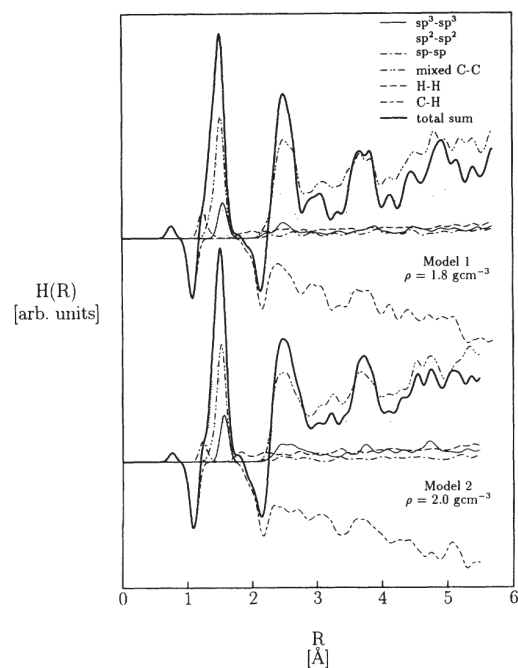
ure 6 also demonstrates the several contributions to the first C-C peak in $G(R)$ from the different parts in the bond length statistics. It is apparent that this peak does not only consist of two Gaussians as is assumed in Paper I, but at least four Gaussian-like contributions could be detected in principle if one includes all the "mixed" C-C bonds into one component. From the comparison of the theoretical and the experimental results we conclude that the "mixed" bonds mainly determine the position of the subpeak at $R = 1.52$ Å. The shoulder representing the other subpeak at $R = 1.34$ Å is predominantly influenced by the π bonds as well as the first C-H correlation that overlaps significantly with the sp-sp contribution. The shoulder in $G(R)$ found in Paper I at $R \approx 1.9$ Å is due to second H-H correlations (H-C-H groups, compare Table II) slightly influenced by the shapes of the first C-C and the second C-H correlations (C-C-H-groups).

V. ELECTRONIC PROPERTIES, CONCLUDING REMARKS

In analyzing the amorphous structures discussed here we have determined the detailed chemical bonding in two a-C:H modifications with slightly different mass density. In relating theoretically simulated structure and diffraction data to experimentally studied a-C:H films, the atomic-scale microstructure in this class of amorphous materials has been elucidated on the molecular level of chemical bonding. A critical assessment of the simulation regime employed here (e.g., quenching of a liquid within small supercell configurations) suggests that we are still far away from complete realization of the quantum-mechanically-based simulation of depo-
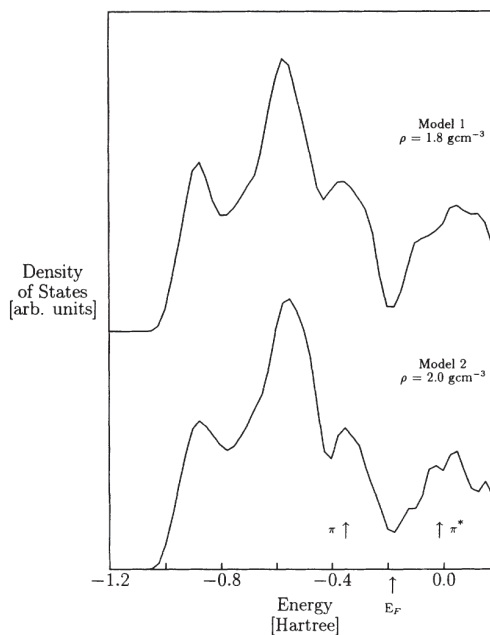

FIG. 6. Hybrid contributions to the radial distribution functions for the two a-C:H models.

FIG. 7. Electronic density of states for the two a-C:H models.

sition processes. This, however, should not discourage such computer modeling experiments', since we can learn more about molecular mechanisms for structure formation, and hence how to control them.

Related to the discussion of chemical bonding in hydrogenated amorphous carbon with a mass density of about $2.0 \ \mathrm{g\,cm^{-3}}$, the corresponding total electronic densities of states has been calculated, as may be seen in Fig. 7. The nature of π-bonded clusters as well as the properties of the remaining matrix (the distribution of clusters and the interconnecting segments), which are determined by the mass density and the hydrogen content, control the energy gap behavior. The TDOS structures are characterized by a clear partition into a low-energy σ-like band built from s and p atomic states, significant π and π^* shoulders below and above the Fermi energy E_F which control the energy gap, and a distinct number of p-like defect states at E_F yielding pseudogap behavior. For models with the mass densities studied here (1.8 and $2.0 \ \mathrm{g/cm^3}$) we obtain a gap width of about 2.6 and 1.9 eV, respectively. These gap values have actually been calculated from the highest occupied molecular orbital–lowest unoccupied molecular orbital (HOMO-LUMO) π-π^* separation of the corresponding zero temperature structures after counting down the defect states around the Fermi level. The relatively small gaps obtained are not caused by the formation of separated more or less extended aromatic ring groupings in the a-C:H structures. They are, rather, a consequence of the smallest π-π^* splitting realized by embedding the local π-electron systems of π-bonded atomic arrangements in a strained bonding environment of a rigid cross-linked network, in which "mixed" bonds dominate.

The correct reproduction of realistic electronic bonding properties and electronic density of state (DOS) behavior, as well as the fundamental reproduction of the scattering properties of amorphous hydrogenated carbon structures, is a basis for a detailed analysis of the bond formation and local defect generation in a-C:H. We find very good agreement between our theories and the experimentally obtained results from elastic and inelastic neutron scattering experiments and from NMR for hard a-C:H samples deposited by a saddle-field ion beam technology. In particular, we support the experimental findings that these amorphous systems predominantly consist of threefold coordinated atoms, which are not arranged in aromatic or graphitelike ring structures, but rather in olefinic groups. We also confirm the existence of sp^3-H and sp^3-H_2 radicals and can demonstrate the existence of H_2 molecules.

ACKNOWLEDGMENTS

[1] G. Galli, R. M. Martin, R. Car, and M. Parrinello, Phys. Rev. B **42**, 7470 (1990).

[2] K. A. Laasonen and R. M. Nieminen, J. Phys. C **2**, 1509 (1990).

[3] J. Tersoff, Phys. Rev. B **37**, 6991 (1988).

[4] D. W. Brenner, Phys. Rev. B **42**, 9458 (1990).

[5] P. C. Kelires, Phys. Rev. B **47**, 1829 (1993).

[6] C. Z. Wang, K. M. Ho, and C. T. Chan, Phys. Rev. Lett. **70**, 611 (1993).

[7] Th. Frauenheim, P. Blaudeck, U. Stephan, and G. Jungnickel, Phys. Rev. B **48**, 4823 (1993).

[8] M. Weiler, R. Kleber, S. Sattel, K. Jung, H. Ehrhardt, G. Jungnickel, S. Deutschmann, U. Stephan, P. Blaudeck, and Th. Frauenheim, Diamond Relat. Mater. **3**, 245 (1994).

[9] G. Jungnickel, M. Kühn, S. Deutschmann, F. Richter, U. Stephan, P. Blaudeck, and Th. Frauenheim, Diamond Relat. Mater. **3**, 1056 (1994).

[10] *Computational Material Sciences*, edited by J. B. Broughton (Elsevier, Amsterdam, in press).

[11] J. K. Walters, P. J. R. Honeybone, D. W. Huxley, R. J. Newport, and W. S. Howells, Phys. Rev. B **50**, 831 (1994).

[12] P. J. R. Honeybone, R. J. Newport, J. K. Walters, W. S. Howells, and J. Tomkinson, Phys. Rev. B **50**, 839 (1994).

[13] C. Jäger, J. Gottwald, H. W. Spiess, and R. J. Newport, Phys. Rev. B **50**, 846 (1994).

[14] P. Blaudeck, Th. Frauenheim, D. Porezag, G. Seifert, and E. Fromm, J. Phys. Condens. Matter **4**, 6389 (1992).

[15] P. Blaudeck, Th. Frauenheim, H.-G. Busmann, and Th. Lill, Phys. Rev. B **49**, 11 409 (1994).

[16] Th. Frauenheim, U. Stephan, P. Blaudeck, D. Porezag, H.-G. Busmann, W. Zimmermann-Ebling, and S. Lauer, Phys. Rev. B **48**, 18 189 (1993).

[17] M. T. Yin and M. L. Cohen, Phys. Rev. Lett. **50**, 2006 (1983).

[18] D. Porezag, S. Uhlmann, Th. Frauenheim, and G. Seifert (unpublished).

[19] G. Jungnickel, M. Haase, Th. Köhler, S. Deutschmann, U. Stephan, P. Blaudeck, and Th. Frauenheim (unpublished).

[20] U. Stephan and M. Haase, J. Phys. Condens. Matter **5**, 9157 (1993).

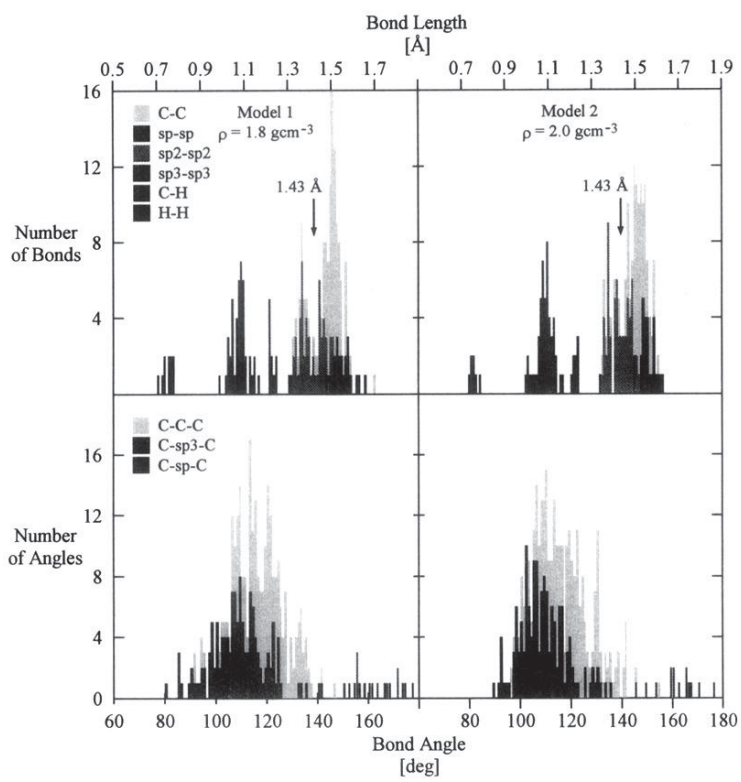[21] D. S. Franzblau, Phys. Rev. B **44**, 4925 (1991).

FIG. 2. Histograms of bond lengths and bond angles for the two model structures.